Copyright © 2011 Tech Science Press MCB, vol.8, no.2, pp.91-104, 2011

# Use of Tensorial Description in Tissue Remodeling: Examples of F-actin Distributions in Pulmonary Arteries in Hypoxic Hypertension

**Wei Huang**[*,†], **Yi Wah Mak**[*] **and Peter C. Y. Chen**[‡§]

**Abstract:** A ***molecular configuration tensor*** $P_{ij}$ was introduced to analyze the distribution of fibrous proteins in vascular cells for studying cells and tissues biomechanics. We have used this technique to study the biomechanics of vascular remodeling in response to the changes of blood pressure and flow. In this paper, the remodeling of the geometrical arrangement of F-actin fibers in the smooth muscle cells in rat's pulmonary arteries in hypoxic hypertension was studied. The rats were exposed to a hypoxia condition of 10% for 0, 2, 12, and 24 hr at sea level. Remodeling of blood vessels were studied at the *in vivo* state under normal perfusion, no-load state when small rings from blood vessels were excised, and zero-stress state after the rings were cut open radially to release the residual stress. Tissue remodeling in response to changes in blood pressure is reflected in the zero-stress state. The tensor components were determined by analyzing the configuration of phalloidin stained F-actin fibers in the media layer of pulmonary arteries. The values of $P_{31}$, $P_{32}$, $P_{33}$ in the *in-vivo state*, the no-load state, and the zero-stress state are obtained. This study demonstrated the distributions of fibrous molecules in tissue remodeling can be described quantitatively using the ***molecular configuration tensor***.

**Keywords:** fibrous protein, tensor, zero-stress state, blood vessel.

## 1 Introduction

This paper is part of a general study in the mechanics of the cells in a blood vessel responding to changes in blood pressure. It has almost been 60 years since the

[*] Department of Health Technology and Informatics, The Hong Kong Polytechnic University, Kowloon, Hong Kong

[†] Correspondent author. E-mail: Wei.Huang@polyu.edu.hk.

[‡] Dept. of Bioengineering, University of California at San Diego, La Jolla, CA 92093-0412

[§] This paper is a tribute to Prof. Pin Tong in honor of his 72th birthday, and edited by Dr. David Lam.

recognition of the DNA's double helix structure. While many scientists are still busy unraveling the behavior of DNA and its interaction with its neighbors, some are interested in understanding how an increase in blood pressure can trigger gene expression resulting in vascular tissue remodeling, such as in hypertension and hypotension.

Regardless of the ultimate objective, we believe an important first step is to understand the geometry of the individual molecules and the geometric structure of the molecular aggregation in the cells and tissues. For this purpose, a second order ***molecular configuration tensor*** $P_{ij}^{g}$ for fibrous protein in the cells and tissues has been defined for quantitative measurement. The subscripts $i, j$ refer to the coordinate axes $x_1, x_2, x_3$, and the superscript $g$ refers to the kind of fibrous protein [Huang (2007)]. Since it is a second order tensor, every molecular configuration tensor $P_{ij}^{g}$ has 9 components: $P_{11}$, $P_{12}$, $P_{13}$, $P_{21}$, $P_{22}$, $P_{23}$, $P_{31}$, $P_{32}$, and $P_{33}$, respectively. As an illustration, the values of 9 components in the molecular configuration tensor for $\alpha$-smooth muscle-actin fibers in rat's abdominal aorta were determined experimentally [Huang, Mak and Chen (2010)]. In this paper, $g$ is for F-actin fibers. The values of $P_{31}, P_{32}, P_{33}$ of F-actin fibers measured in the smooth muscle cells of the pulmonary arteries at *in vivo* state, no-load state, and zero-stress state of vessel wall tension were reported.

In this paper, we consider a normal rat lung subjected to lowered oxygen concentration in the breathing gas. The oxygen tension was lowered from 20.9% to 10% as a step function of time, i.e., lowered at time 0 and then kept constant afterwards. We have reported the physiological functional parameters of the rat lung in response to the increase in blood pressure when breathing a hypoxic gas mixture. Results contained details of the history of the blood pressure, the diameter of the pulmonary arteries, the wall thickness of the pulmonary arteries, the opening angle that described the zero-stress state of the arteries, and the elastic moduli of the arteries [Huang, Shen, Huang and Fung (1998); Huang, Shen, Huang and Fung (1999); Huang, Sher, Delgado-West, Wu and Fung (2001); Huang, Delgado-West, Wu and Fung (2001)]. In addition, we have reported the gene expressions as functions of time and oxygen concentration measured with a microarray colorimetric method, and compared the gene expression function with those of the physiological functional parameters, and the comparison yielded a quantitative measure or correlation between the gene and physiology [Huang, Sher, Peck and Fung (2002)].

Vascular endothelial cells, smooth muscle cells, and fibroblasts in blood vessel wall are exposed to dynamic stretching and shearing due to blood pressure and blood flow. As stress and strain are imposed on the vascular cells, a growing body of evidence has indicated that the cytoskeleton, including actin, microtubules, and intermediate filaments, plays a major role in transmitting and distributing mechanical

stresses within the cell, as well as in their conversion into biochemical responses [Chien (2007)].

In this paper, the remodeling of the geometrical arrangement of F-actin fibers in the smooth muscle cells in rat's pulmonary arteries in hypoxic hypertension was studied.

## 2 Materials and Methods

Thirty-two male Sprague Dawley rats (Harlan, San Diego, CA), 351 $\pm$ 8 g body weight, raised in normal air at sea level, were used in this study. The protocol was approved by the University of California, San Diego Committee on Animal Research.

We studied the tissue remodeling of pulmonary arteries in hypoxic hypertension in rats. In order to change the blood pressure in rat lung, the rats living in a modified commercially available animal chamber (Snyder, Denver) were subjected to a sudden decrease in oxygen concentration from 20.9% to 10% in the chamber, and then remained at 10% for 0, 2, 12, or 24 hr. The size of the chamber was 0.28 $m^3$ ($0.66 \times 0.56 \times 0.75$). The change in oxygen concentration level from 20.9 to 10% was accomplished in $1.5 \pm 0.5$ min by an infusion of pure $N_2$ at a selected rate that was well mixed with room air using a fan. A feedback control system with $O_2$ sensor and a flow meter for $N_2$ was used. $CO_2$ in the hypoxic chamber was absorbed by soda lime (Fisher Scientific), and ammonia was absorbed by activated carbon (Fisher Scientific). For monitoring the oxygen concentration in the chamber, we used a portable oxygen analyzer (Model 320A, Teledyne Analytical Instruments, City of Industry, CA) with a flow-through adapter in the animal cage.

At any scheduled time, a rat was removed from the hypoxic chamber, and anesthetized immediately with an intraperitoneal injection of pentobarbital sodium (50 mg/kg body weight). The trachea was cannulated, and both lungs were partially inflated at 10 cm $H_2O$. Bilateral thoracotomy was performed. After a bolus of normal saline with 1000 U/kg body weight of heparin (1000 U/ml) was injected, the blood in cardiovascular system was washed out by vascular perfusion of 0.1 M physiological saline buffer (PBS) for 30 min under a perfusion pressure of 80 mm Hg in the left ventricle and a draining pressure of 0 mm Hg at the left atrium while the lungs were inflated at 10 cm $H_2O$. Then left main pulmonary arteries (order 11, or region 2, according to our previous study in [Huang, Sher, Delgado-West, Wu and Fung (2001)] between the conjunction of left and right pulmonary arteries and the third side branch were collected at three different states: *in vivo* state, no-load state, and zero-stress state, respectively, as described in the following.

The tissue samples at *in vivo* state were prepared after the pulmonary arteries were

fixed *in situ* by vascular perfusion of 4 percent formaldehyde in 0.1 M physiological saline buffer (PBS) for 30 min under a perfusion pressure of 80 mm Hg in the left ventricle and a draining pressure of 0 mm Hg at the left atrium while the lungs were inflated at 10 cm $H_2O$. Then the tissue samples were harvested and kept in 4 percent formaldehyde in 0.1 M PBS overnight. The tissue samples at no-load state were prepared after the blood vessel specimens were cut into small rings and fixed in 4 percent formaldehyde in 0.1 M PBS overnight. The tissue samples at zero-stress state were prepared after the small vascular rings were cut radially into sectors in order to release the residual stress in the wall, then the sectors were fixed in 4 percent formaldehyde in 0.1 M PBS overnight. The orientation of all tissue specimens was marked by referring to the blood flow direction. In **Figure 1A**, the upper figure shows a blood vessel with flow, the lower figure shows a schematic drawing of the endothelium. A Cartesian coordinate system is shown with $x_1$-axis parallel to the direction of blood flow, $x_3$-axis perpendicular to the basal lamina, and $x_2$-axis normal to $x_1$ and $x_3$. **Figure 1B** shows the cross-sectional view of a pulmonary artery (inner diameter: 92 $\mu$m, mean wall thickness: 84 $\mu$m) stained with toluidine blue O. The endothelium, media, and adventitia layers of the artery are marked.

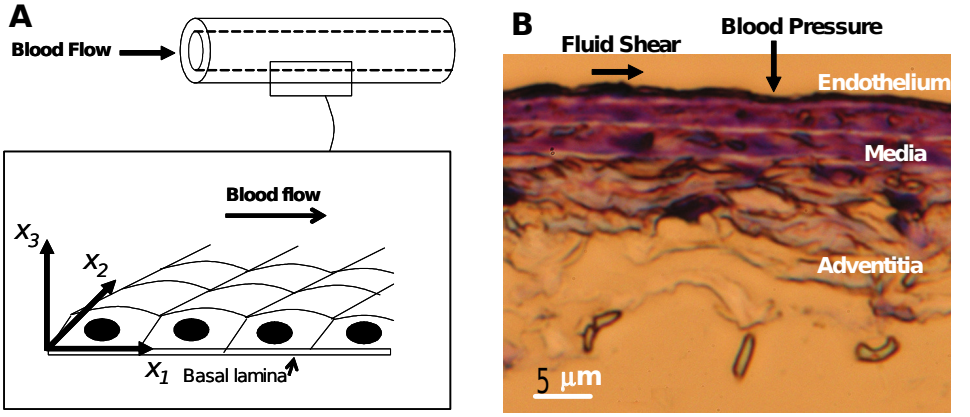


Figure 1: (A) A schematic drawing of a blood vessel with the direction of blood flow in the upper figure, and a magnified schematic drawing of the endothelium with a longitudinal cross section in the front in the lower figure. A Cartesian coordinate system with $x_1$-axis parallel to the direction of blood flow, $x_3$-axis perpendicular to the basal lamina, and $x_2$-axis normal to $x_1$ and $x_3$ is used as references to label the endothelium. (B) The cross-sectional view of a pulmonary artery shows the intima (including endothelium and basal lamina), media, and adventitia layers.

The fibrous actin fibers in the pulmonary arterial smooth muscle cells (media layer in **Fig. 1B**) at *in vivo* state, no-load state, and zero-stress state were stained with phalloidin (Alexa Fluor 488 phalloidin, Molecular Probes, Eugene, OR) following the protocol described in [Huang (2007)]. The fluorescence stained specimens were placed on microscope slides (Superfrost Plus GOLD) with the endothelium facing up, and mounted with ProLong Gold antifade regent (Molecular Probes). A #1.5 micro cover glass (Thamos Scientific) was placed on top of the endothelium, and the edges of the cover glass were sealed with nail polish. The specimens were then observed with a confocal scanning microscope (Model 10, Yokogawa, Tokyo, Japan), with a set of fluorescence filters (Excitation: 488 nm, Emission: 525 nm, Band Width: 50 nm). A 60$\times$ 1.45 NA plan apo oil immersion objective was used. The refraction index of the immersion oil was 1.516. The calibration value for our set-up was 9.13 pixels/$\mu$m. The thickness of an optical section was 0.2 $\mu$m. By stepping the objective through the thickness of the specimen in the direction of the $x_3$-axis that was perpendicular to the endothelium, the endothelium and the smooth muscle layer were identified. The 2-dimensional images in $x_3$-axis were taken with one of the image edges perpendicular to the blood flow direction in the blood vessel. Fluorescent images were taken in successive planes, and captured with a Hamamatsu digital camera (model: ORCA-ER, Hamamatsu Photonics, Hamamatsu, Japan). Images were taken for the strips without fluorescence staining to be used as controls. Digitized images were acquired using the Simple PCI imaging software (Compix Inc., Cranberry Township, Pennsylvania) and saved for image analysis.

**Figure 2** shows four examples of the different geometrical arrangements of F-actin fibers in the smooth muscle cells of the pulmonary arteries at *in vivo* state of vessel wall tension. The vascular smooth muscle cells were prepared when the pulmonary arteries were fixed with 4% formaldehyde in phosphate buffer solution at *in vivo* state (80 mm Hg at left ventricle, and 0 mm Hg at left atrium) after the rats were exposed to a hypoxia of 10% for 0 (**Fig. 2A**), 2 (**Fig. 2B**), 12 (**Fig. 2C**), or 24 hr (**Fig. 2D**), respectively.

**Figure 3** shows the different geometrical arrangements of F-actin fibers in the smooth muscle cells of the pulmonary arteries at no-load state of vessel wall tension in 4 examples. The vascular smooth muscle cells were prepared when the pulmonary arteries were fixed with 4% formaldehyde in phosphate buffer solution at no-load state after the rats were exposed to a hypoxia of 10% for 0 (**Fig. 3A**), 2 (**Fig. 3B**), 12 (**Fig. 3C**), or 24 hr (**Fig. 3D**), respectively.

**Figure 4** shows the different geometrical arrangements of F-actin fibers in the smooth muscle cells of the pulmonary arteries at zero-stress state of vessel wall tension in 4 examples. The vascular smooth muscle cells were prepared when the

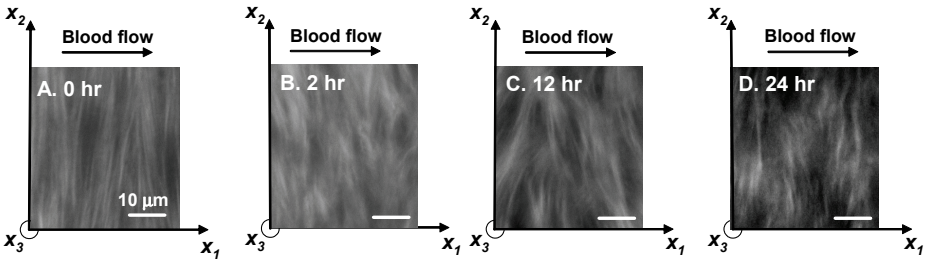


Figure 2: Plan views of the vascular smooth muscle cells in rat's pulmonary artery at *in vivo* state. The vascular smooth muscle cells were prepared when the pulmonary arteries were fixed with 4% formaldehyde in phosphate buffer solution at *in vivo* state (80 mm Hg at left ventricle, and 0 mm Hg at left atrium) after the rats were exposed to a hypoxia of 10% for 0 (**A**), 2 (**B**), 12 (**C**), or 24 hr (**D**), respectively. $x_1$, the longitudinal axis of the vessels in the blood flow direction; $x_2$, the circumferential direction; $x_3$, the radial direction.

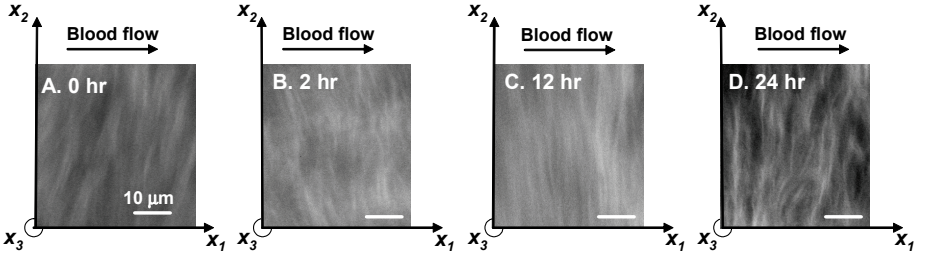


Figure 3: Plan views of the vascular smooth muscle cells in rat's pulmonary artery at no-load state. The vascular smooth muscle cells were prepared when the pulmonary arteries were fixed with 4% formaldehyde in phosphate buffer solution at no-load state after the rats were exposed to a hypoxia of 10% for 0 (**A**), 2 (**B**), 12 (**C**), or 24 hr (**D**), respectively. $x_1$, the longitudinal axis of the vessels in the blood flow direction; $x_2$, the circumferential direction; $x_3$, the radial direction.

pulmonary arteries were fixed with 4% formaldehyde in phosphate buffer solution at zero-stress state after the rats were exposed to a hypoxia of 10% for 0 (**Fig. 4A**), 2 (**Fig. 4B**), 12 (**Fig. 4C**), and 24 hr (**Fig. 4D**), respectively.

The digitized images of the F-actin fibers on the layer of smooth muscle cells under the endothelium were analyzed and measured with the MetaMorph Imaging system

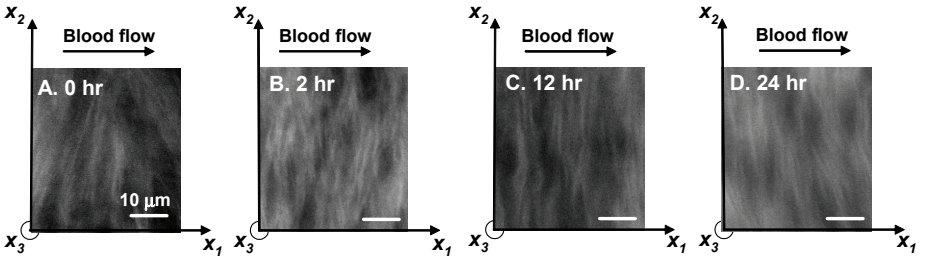


Figure 4: Plan views of the vascular smooth muscle cells in rat's pulmonary artery at zero-stress state. The vascular smooth muscle cells were prepared when the pulmonary arteries were fixed with 4% formaldehyde in phosphate buffer solution at zero-stress state after the rats were exposed to a hypoxia of 10% for 0 (**A**), 2 (**B**), 12 (**C**), or 24 hr (**D**), respectively. $x_1$, the longitudinal axis of the vessels in the blood flow direction; $x_2$, the circumferential direction; $x_3$, the radial direction.

(Version: 6.3 r2, Universal Imaging Corporation, Downingtown, PA). In analyzing the images, all F-actin fibers as shown in **Figures 2-4** were assumed as vectors going from left to right. The images of the phalloidin-stained F-actin fibers in the computer yielded data on the orientation $\theta$, width $h$, and length $L$ of F-actin fibers in the smooth muscle cells in the plan view as shown in **Figs. 2-4**. **Figure 5** illustrates the steps to describe the geometric distribution of the F-actin fibers. The detailed procedures on measuring $P^g_{ij}$ tensor were described in [Huang (2007)].

Based on these measurements, the values of $P_{31}, P_{32}, P_{33}$ in the $P^g_{ij}$ tensor of F-actin in the smooth muscle cells as shown in **Figures 2-4** were computed by

$$P^g_{ii} = \frac{1}{A}\sum \textit{area of the dots}, \tag{1}$$

$$P^g_{ij} = \frac{1}{A}\sum hL_j, \tag{2}$$

$$P^g_{ik} = \frac{1}{A}\sum hL_k, \tag{3}$$

where $i, j, k$ = 1, 2, or 3, $A$ is an area of the rectangle of the figures , $h$ is the width and $L$ is the length of F-actin fibers in the smooth muscle cells in the plan view.

In this paper, the values of $P_{31}, P_{32}, P_{33}$ of F-actin fibers measured in the smooth muscle cells of the pulmonary arteries at *in vivo* state, no-load state, and zero-stress state of vessel wall tension were reported.

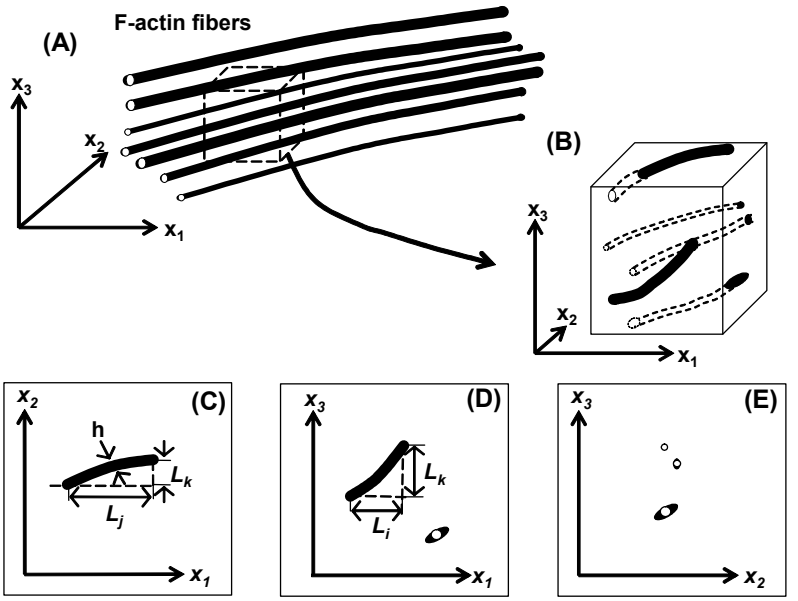


Figure 5: A scheme to describe how to measure the ***molecular configuration tensor*** of F-actin fibers [Huang (2007)].

## 3 Results

### *3.1 Values of $P_{31}$, $P_{32}$, $P_{33}$ of F-actin fibers measured in the smooth muscle cells of the pulmonary arteries at in vivo state of vessel wall tension*

The results in **Figure 2** are: in **Fig. 2A**, $P_{31}$ is 0.025, $P_{32}$ is 0.077, $P_{33}$ is 0; in **Fig. 2B**, $P_{31}$ is 0.054, $P_{32}$ is -0.189, $P_{33}$ is 0; in **Fig. 2C**, $P_{31}$ is 0.089, $P_{32}$ is -0.135, $P_{33}$ is 0; in **Fig. 2D**, $P_{31}$ is 0.047, $P_{32}$ is 0.108, $P_{33}$ is 0.

At each time point, 4 samples were analyzed to obtain the mean value and standard deviation. A total of 16 samples were studied for the time points of 0, 2, 12, and 24 hr, respectively. The mean value and standard deviation of $P_{31}$ are: 0.042 $\pm$0.031 at 0 hr, 0.052$\pm$0.018 at 2 hr, 0.050$\pm$0.027 at 12 hr, and 0.048$\pm$0.010 at 24 hr, respectively. The mean value and standard deviation of $P_{32}$ are: -0.003 $\pm$0.231 at 0 hr, 0.002$\pm$0.131 at 2 hr, 0.031$\pm$0.115 at 12 hr, and -0.009$\pm$0.144 at 24 hr, respectively. All $P_{33}$ values are zero. One-way ANOVA analysis was performed, and the differences of $P_{31}$ and $P_{32}$ among different time points were not significant.

### 3.2 Values of $P_{31}$, $P_{32}$, $P_{33}$ of F-actin fibers measured in the smooth muscle cells of the pulmonary arteries at no-load state of vessel wall tension

The values of $P_{31}$, $P_{32}$, $P_{33}$ in **Figure 3** are: in **Fig. 3A**, $P_{31}$ is 0.054, $P_{32}$ is 0.113, $P_{33}$ is 0; in **Fig. 3B**, $P_{31}$ is 0.081, $P_{32}$ is -0.128, $P_{33}$ is 0; in **Fig. 3C**, $P_{31}$ is 0.040, $P_{32}$ is -0.046, $P_{33}$ is 0; in **Fig. 3D**, $P_{31}$ is 0.032, $P_{32}$ is 0.081, $P_{33}$ is 0.

A total of 16 samples were analyzed for the time points of 0, 2, 12, and 24 hr, respectively, with 4 samples per time point. The mean value and standard deviation of $P_{31}$ are: 0.044 $\pm$0.016 at 0 hr, 0.067$\pm$0.010 at 2 hr, 0.071$\pm$0.026 at 12 hr, and 0.070$\pm$0.033 at 24 hr, respectively. The mean value and standard deviation of $P_{32}$ are: -0.072$\pm$0.051 at 0 hr, -0.049$\pm$0.141 at 2 hr, -0.086$\pm$0.067 at 12 hr, and -0.001$\pm$0.079 at 24 hr, respectively. All $P_{33}$ values are zero. One-way ANOVA analysis was performed. The differences of $P_{31}$ and $P_{32}$ among different time points were not significant.

### 3.3 Values of $P_{31}$, $P_{32}$, $P_{33}$ of F-actin fibers measured in the smooth muscle cells of the pulmonary arteries at zero-stress state of vessel wall tension

The values of $P_{31}$, $P_{32}$, $P_{33}$ in **Figure 4** are: in **Fig. 4A**, $P_{31}$ is 0.050, $P_{32}$ is 0.009, $P_{33}$ is 0; in **Fig. 4B**, $P_{31}$ is 0.043, $P_{32}$ is 0.024, $P_{33}$ is 0; in **Fig. 4C**, $P_{31}$ is 0.030, $P_{32}$ is -0.025, $P_{33}$ is 0; in **Fig. 4D**, $P_{31}$ is 0.078, $P_{32}$ is -0.145, $P_{33}$ is 0.

A total of 16 samples were analyzed for the time points of 0, 2, 12, and 24 hr, respectively, with 4 samples per time point. The mean value and standard deviation of $P_{31}$ are: 0.062 $\pm$0.026 at 0 hr, 0.044$\pm$0.002 at 2 hr, 0.035$\pm$0.007 at 12 hr, and 0.056$\pm$0.017 at 24 hr, respectively. The mean value and standard deviation of $P_{32}$ are: -0.021$\pm$0.072 at 0 hr, -0.011$\pm$0.051 at 2 hr, -0.078$\pm$0.044 at 12 hr, and -0.102$\pm$0.053 at 24 hr, respectively. All $P_{33}$ values are zero. One-way ANOVA analysis was done. The differences of $P_{31}$ and $P_{32}$ among different time points were not significant.

## 4 Discussion

Low oxygen concentration in the breathing gas, or hypoxia, at high altitude and in some lung diseases leads to hemodynamic and anatomical changes in the pulmonary circulation [Meyrick and Reid (1978); Sobin, Tremer, Hardy and Chiodi (1983); von Euler and Liljestrand (1946); Wagner and Weir (1994); West (1998); Yuan (2004)], as well as the changes of lung tissues in cellular and molecular levels [Yuan (2004)]. F-actin fiber is one of the important cytoskeletons in the endothelial cells, and transduces extracellular forces into stresses in the cell interior [Chien (2007); Hu, Chen, Fabry, Numaguchi, Gouldstone, Ingber, Fredberg, Butler and Wang (2003); Mofrad and Kamm (2006); Galbraith, Skalak and Chien (1998)]. In

this paper, the $P_{31}$, $P_{32}$, $P_{33}$ values in the $P^g_{ij}$ tensor of F-actin fiber in the smooth muscle cells of the pulmonary arteries at *in vivo* state, no-load state, and zero-stress state of vessel wall tension, and their changes during tissue remodeling were determined. The other values in the $P^g_{ij}$ tensor in vascular remodeling are under investigations. The $P^g_{ij}$ tensor provides us a tool to study the cellular molecules in the tissue remodeling of blood vessels.

A measurable molecular configuration tensor $P^g_{ij}$ for fibrous protein in the cells and tissues is usually the result of complex molecular interactions in cells and tissues. The molecular geometry is the foundation of the mechanical properties of the molecular aggregates. The mechanical properties of the molecular aggregates are the foundation of the physical behavior of the cells and tissues. Following this reasoning, we see that it is important to clarify the geometric structure of the aggregation of these molecules. The molecular configuration tensor $P^g_{ij}$ for fibrous protein provides a tool for achieving this goal. When the geometric information becomes available, the mechanics of the molecules can be embodied in the constitutive equation. Since both stress and strain tensors are of rank 2 in all available constitutive equations, we expect a second order molecular configuration tensor $P^g_{ij}$. With a valid constitutive equation it is possible to predict cellular behavior under stress and characterize cellular growth, injury and repair processes.

In biomechanics, the constitutive equations link the equations of equilibrium and motion and the boundary conditions to the anatomy, histology, physiology, and biochemistry of the system. There are different forms of constitutive equations in biomechanics. The mechanics of tissue remodeling stands out as a large subset of the literature [Abé, Hayashi and Sato (1996); Fung and Tong (2001); Chuong and Fung (1983); Liu and Fung (1992); Danescu (1997); Humphrey (1999); Huyghe and Janssen (1997); May-Newman and Yin (1998); Rachev (1997); Vaishnav, Vossoughi, Patel, Cothran, Coleman and Ison-Franklin (1990); Weber, Stergiopulos, Brunner and Hayoz (1996); Zanchi, Stergiopulos, Brunner and Hayoz (1998); Zeller and Skalak (1998)]. In tissues, force and stress cannot be photographed, but must be inferred from logic and mathematics. The most important tool to visualize stress is to use the Hooke's law of simple elastic solids. For a more complex solid, Hooke's law gives way to a more complex stress-strain relationship, or constitutive equation. The materials of the blood vessel wall of interest to us are shown in **Figure 1**, which is a cross-sectional view of a pulmonary artery.

If the strains were finite, then the stress-strain relationship is nonlinear because of the kinematics of finite displacement. Most nonlinear theories in the literature are concerned with finite strains. For relatively small ranges of the strain, it is expedient to use linear approximations. The literature on the stress-strain relationship and the data on elastic moduli of arteries collected up to 1996 has been collated and

reviewed in a book by Abé, Hayashi and Sato (1996). There are different forms of constitutive equations in biomechanics. A penetrating analysis of the theories, experimentation, methodology, and interpretation of results in arterial mechanics was presented by Humphrey (1999).

Blood vessels are constantly exposed to cyclic stretching and shearing due to blood pressure and blood flow, and remodel in response to the changes of the mean blood pressure or mean blood flow in health and disease. Cells respond to pressure, flow, and stretch. The cytoskeleton is composed of three filamentous systems: microfilaments (made up mainly of actin and myosin), intermediate filaments, and microtubules. The role of vascular cells in vascular remodeling is controlled by both mechanical stresses and chemical factors (such as nitric oxide, ion channels, and growth factors). The mechanics of the molecular basis is of obvious importance, and is awaiting clarification. Many scientists have focused on the molecules in the vascular cells related to the shear stress of fluid flow acting on the cell wall [Chien (2007)]. Attention had been focused on the identification of these molecules. How do these molecules affect the mechanical properties of the cells is a question that has not received much attention. So far none of the existing constitutive equations includes attention to the molecular configuration. We are just making a beginning on this line of inquiry.

In summary, the remodeling of the geometrical arrangement of F-actin fibers in the vascular smooth muscle cells was studied. The values of $P_{31}, P_{32}, P_{33}$ in the molecular configuration tensor $P^g_{ij}$ of F-actin fibers in the vascular smooth muscle cells in rat's pulmonary arteries were obtained at three different states: *in vivo* state, no-load state, and zero-stress state. The rats were exposed to 10% hypoxia for 0, 2, 12, or 24 hr, respectively. The differences of $P_{31}$ and $P_{32}$ among four different time points were not significant at *in vivo* state, no-load state, and zero-stress state, respectively. Further investigations are under way.

**Acknowledgement:** This study was supported by the National Foundation of Science Grant CMS-0626438, and the Hong Kong Polytechnic University start-up fund 1-55-56-99EZ and initial grant A.55.37.PJ35 to Wei Huang.

## References

1. Abé, H.; K. Hayashi; M. Sato. (eds) (1996): Data Book on Mechanical Properties of Living Cells, Tissues, and Organs. Spriner, Tokyo.

2. Chien, S. (2007): Mechanotransduction and endothelial cell homeostasis: the wisdom of the cell. *Am J Physiol Heart Circ Physiol.* 292: 1209-1224.

3. Chuong, C. J.; Fung, Y. C. (1983): Three-dimensional stress distribution in arteries. *J Biomech Eng.* 105: 268-274.

4. Danescu, A. (1997): The number of elastic moduli for anisotropic polynomial constitutive equations. *Mech. Res. Commun*. 24: 289-302.

5. Fung, Y. C.; Tong, P. (2001): *Classical and Computational Solid Mechanics*. World Scientific Publishing, Singapore.

6. Galbraith, C. G.; Skalak, R.; Chien, S. (1998): Shear stress induces spatial reorganization of the endothelial cell cytoskeleton. *Cell Motil Cytoskeleton* 40, 317-330.

7. Hu, S.; Chen, J.; Fabry, B.; Numaguchi, Y.; Gouldstone, A.; Ingber, D. E.; Fredberg, J. J.; Butler, J. P.; Wang, N. (2003): Intracellular stress tomography reveals stress focusing and structural anisotropy in cytoskeleton of living cells. *Am J Physiol Cell Physiol* 285: C1082-C1090.

8. Huang, W. (2007): Tensorial description of the geometrical arrangement of the fibrous molecules in vascular endothelial cells. *Molecular & Cellular Biomechanics*, 4: 119-131.

9. Huang, W.; Mak, Y. W.; Chen, P. C. Y. (2010): Application of tensorial description of the fibrous molecules geometrical arrangement in vascular tissues and cells. *International Federation for Medical and Biological Engineering Proceedings* 31, 875–878.

10. Huang, W.; Shen, Z.; Huang, N. E.; Fung, Y. C. (1998): Use of intrinsic modes in biology: Examples of indicial response of pulmonary blood pressure to step hypoxia, *Proc. Natl. Acad. Sci.* USA 95: 12766–12 771.

11. Huang, W.; Shen, Z.; Huang, N. E.; Fung, Y. C. (1999): Nonlinear indicial response of complex nonstationary oscillations as pulmonary hypertension responding to step hypoxia. *Proc. Natl. Acad. Sci. USA* 96: 1834–1839.

12. Huang, W.; Sher, Y. P.; Delgado-West, D.; Wu, J. T.; Peck, K.; Fung, Y. C. (2001): Tissue remodeling of rat pulmonary artery in hypoxic breathing: I. Changes of morphology, zero-stress state and gene expression, *Ann. Biomed. Eng.* 29: 535-551.

13. Huang, W.; Delgado-West, D.; Wu, J. T.; Fung, Y. C. (2001): Tissue remodeling of rat pulmonary artery in hypoxic breathing: II. Course of change of mechanical properties, *Ann. Biomed. Eng.* 29: 552-562.

14. Huang, W.; Sher, Y. P.; Peck, K.; Fung, Y. C. (2002): Matching gene activity with physiological functions. *Proc. Natl Acad. Sci. USA* 99: 2603-2608.

15. Humphrey, J. (1999): An evaluation of psuedoelastic descriptors used in arterial mechanics. *J. Biom. Engin.* 121: 259-262.

16. Huyghe, J. M.; Janssen, J. D. (1997): Quadriphasic mechanics of swelling incompressible porous media. *Int. J. Engng Sci.,* 35: 793-802.

17. Liu, S. Q.; Fung, Y. C. (1992): Influence of STZ-induced diabetes on zero-stress states of rat pulmonary and systemic arteries. *Diabetes*, 41: 136-146.

18. May-Newman, K.; Yin, F. C. P. (1998): A Constitutive Law for Mitral Valve Tissue. *J. of Biomech. Eng.* 120: 38-47.

19. Meyrick, B.; Reid, L. (1978): The effect of continued hypoxia on rat pulmonary arterial circulation: An ultrastructural study, *Lab. Invest.* 38: 188–200.

20. Mofrad, R. K.; Kamm, R. D. (Eds.) (2006):: Cytoskeletal Mechanics: models and measurements. Cambridge University Press, 244 pages, New York, NY.

21. Rachev, A. (1997): Theoretical study of the effect of stress-dependent remodeling on arterial geometry under hypertensive conditions. *J Biomech.* 30: 819-827.

22. Sobin, S. S.; Tremer, H. M.; Hardy, J. D.; Chiodi, H. P. (1983): Changes in arteriole in acute and chronic hypoxic pulmonary hypertension and recovery in rat, *J. Appl. Physiol.* 55: 1445–1455.

23. Vaishnav, R. N.; Vossoughi, J.; Patel, D. J.; Cothran, L. N.; Coleman, B. R.; Ison-Franklin, E. L. (1990): Effect of hypertension on elasticity and geometry of aortic tissue from dogs. *J Biomech Eng.* 112: 70-74.

24. von Euler, V. S.; Liljestrand, G. (1946): Observations on the pulmonary arterial blood pressure in the cat, *Acta Physiol. Scand.* 12: 301–320.

25. Wagner, W. W., Jr.; Weir, E. K. (eds) (1994): *The Pulmonary Circulation and Gas Exchange*, Futura Pub. Co., Armonk, NY.

26. Weber, R.; Stergiopulos, N.; Brunner, H. R.; Hayoz, D. (1996): Contributions of vascular tone and structure to elastic properties of a medium-sized artery. *Hypertension* 27: 816-822.

27. West, J. B. (1998): *High Life: A History of High-Altitude Physiology and Medicine*, Oxford University Press, New York, NY.

28. Yuan, J. X.-J. (ed.) (2004): *Hypoxic pulmonary vasoconstriction: Cellular and Molecular Mechanisms.* Kluwer Academic Publishers, Boston, MA.

29. Zanchi, A.; Stergiopulos, N.; Brunner, H. R.; Hayoz, D. (1998): Differences in the mechanical properties of the rat carotid artery in vivo, in situ, and in vitro. *Hypertension* 32: 180-185.

30. Zeller, P. J.; Skalak, T. C. (1998): Contribution of individual structural components in determining the zero-stress in small arteries. *J Vasc Res.* 35: 8-17.